

1

Prediction of survival after hepatectomy using a physiologically based pharmacokinetic model of indocyanine green liver function tests

Adrian Köller¹, Jan Grzegorzewski¹, Michael Tautenhahn² and Matthias König^{1,*}

¹ Institute for Theoretical Biology, Institute of Biology, Humboldt University, Berlin, Germany

² Experimental Transplantation Surgery, Department of General, Visceral and Vascular Surgery, Jena University Hospital, Jena, Germany

Correspondence*:

Matthias König
koenigmx@hu-berlin.de

2 ABSTRACT

The evaluation of hepatic function and functional capacity of the liver are essential tasks in hepatology, especially in the context of liver surgery. Indocyanine Green (ICG) is a widely applied test compound that is used in clinical routine to evaluate hepatic function. Important questions for the functional evaluation with ICG in the context of hepatectomy are how liver disease such as cirrhosis alters ICG elimination, and if postoperative survival can be predicted from preoperative ICG measurements. Within this work a physiologically based pharmacokinetic (PBPK) model of ICG pharmacokinetics was developed and applied to the prediction of liver resection under various degrees of cirrhosis. For the parametrization of the computational model and validation of model predictions a database of ICG pharmacokinetic data was established. The model was applied (i) to study the effect of liver cirrhosis and hepatectomy on ICG pharmacokinetics; and (ii) to evaluate model-based prediction of postoperative ICG-R15 as a measure for postoperative outcome. Key results were that the model is able to accurately predict changes in ICG pharmacokinetics caused by liver cirrhosis and postoperative changes of ICG-elimination after liver resection, as validated with a wide range of data sets. Based on the PBPK model predictions a classifier allowed to predict survival after hepatectomy, demonstrating its potential value as a clinical tool.

Keywords: Indocyanine Green, Hepatectomy, Liver Cirrhosis, Mathematical Model, Computational Model, Pharmacokinetics, Liver Function, Liver Resection

1 INTRODUCTION

Determining liver function is a crucial task in hepatology, e.g., for diagnostics of liver disease or evaluating pre- and postoperative functional capacity of the liver. Accurate evaluation is especially relevant in the context of liver surgery as postoperative complications are often associated with reduced functional capacity. Comprehensive characterization of the status of a patient and their liver are performed before liver surgery such as hepatectomy. This includes among others anthropometric factors (e.g. age, sex, body weight), static liver function tests (e.g., ALT, AST, albumin, bilirubin, INR, prothrombin time), cardiovascular

parameters (e.g. cardiac output, blood pressure, hepatic blood flow) and lifestyle factors (e.g. smoking, medication). In addition CT scans are performed for planning of the operation. An important method for quantitative evaluation of liver function are pharmacokinetic measurements of test compounds specifically metabolized by the liver (dynamical liver function tests) such as methacetin (LiMAX (Rubin et al., 2017) and MBT (Gorowska-Kowolik et al., 2017)), caffeine (Renner et al., 1984) or galactose (Bernstein et al., 1960).

Indocyanine green (ICG) is such a test compound that is widely used to assess hepatic function. ICG is an inert, anionic, water-soluble, tricarbocyanine dye that is immediately bound to plasma proteins after intravenous administration. ICG is taken up exclusively by the liver and excreted unchanged into the bile. It is not reabsorbed by the intestine and does not undergo enterohepatic circulation (Wheeler et al., 1958). ICG is an ideal test compound to test hepatic uptake and biliary excretion. Determining liver function using ICG is based on its plasma-concentration time course after administration. Based on the time course pharmacokinetic parameters are calculated, with the most commonly used parameters being: (i) ICG retention ratio 15 minutes after administration (ICG-R15) [%]; (ii) ICG plasma disappearance rate (ICG-PDR) [%/min]; (iii) ICG-clearance [ml/min]; and (iv) ICG half-life (ICG-t_{1/2}) [min]. Reduced elimination of ICG by the liver is directly reflected by these parameters (Sakka, 2018).

Liver disease, especially advanced and more severe liver disease, is accompanied by a loss of liver function which can be quantified with dynamical liver function tests. The effects of liver disease on ICG-elimination have been studied extensively, e.g., in different stages of primary biliary cholangitis (PBC) (Vaubourdolle et al., 1991). ICG elimination is reduced in Gilbert's disease (Martin et al., 1976) as well as in patients with hepatic fibrosis and cirrhosis (Gadano et al., 1997). Interestingly, also non-liver diseases can affect ICG parameters, e.g., ICG-clearance is significantly reduced in patients with chronic pancreatitis (Andersen et al., 1999).

Liver cirrhosis is the final stage of many liver diseases and highly relevant in the context of liver surgery. The most common causes are alcoholism, chronic hepatitis C virus infection or non-alcoholic fatty liver disease (Hackl et al., 2016). The pathological characteristics of liver cirrhosis include degeneration of hepatocytes as well as a reduction of liver perfusion through increased portal resistance. Additionally, intrahepatic shunts form, which bypass a portion of the liver blood supply around the functioning liver tissue. From the shunted blood, no ICG can be extracted by the liver, resulting in further reduced elimination (Schuppan and Afdhal, 2008).

The severity of cirrhosis can be described using the Child-Turcotte-Pugh- Score (CTP) (Child and Turcotte, 1964; Pugh et al., 1973). The CTP is an empiric, qualitative, dis-continuous classification of the severity of the "hepatic functional reserve" (Botero and Lucey, 2003). Based on a set of parameters, the CTP assigns a score from 5-15 to a cirrhotic patient, where the more severe a patients symptoms are the higher the score is. These parameters are serum bilirubin and albumin concentrations, pro-thrombin time, the International Normalized Ratio (INR) and the existence of ascites (increased amount of fluid in the peritoneal cavity due to liver cirrhosis) (Child and Turcotte, 1964; Pugh et al., 1973). Patients are classified as CTP-A (5-6 points, low risk), CTP-B (7-9 points, intermediate risk) or CTP-C (10-15 points, high risk). Differences in ICG-elimination between cirrhotic patients and control subjects has been widely assessed (Caesar et al., 1961; Burns et al., 1991; Gilmore et al., 1982; Figg et al., 1995; Møller et al., 2019; Mukherjee et al., 2006; Pind et al., 2016). A good correlation between CTP-score and ICG-elimination has been reported with ICG-elimination decreasing as CTP-score increases (Figg et al., 1995; Møller et al., 2019; Mukherjee et al., 2006; Pind et al., 2016). For many liver diseases, liver surgery is the only effective treatment with hepatectomy being the most common. Liver resection (hepatectomy) describes the removal

70 of part of the liver. Hepatectomy is the most important procedure in liver surgery with more than 20,000
71 liver resections in Germany per year (Filmann et al., 2019). It has been widely performed for the treatment
72 of various liver diseases, such as malignant tumors, benign tumors, calculi in the intrahepatic ducts, hydatid
73 disease, and abscesses (Jin et al., 2013). Despite advances in technology and high experience of liver
74 resection of specialized centers, postoperative morbidity and mortality is still a major issue. Especially,
75 complex resections are being more and more performed in older and high risk patient population (Jin et al.,
76 2013)

77 Major hepatectomy in the presence of cirrhosis is considered to be contraindicated due to the high
78 mortality rate. Recommendations are often that only selected patients with Child's A status or ICG-R15 of
79 less than 10% undergo major hepatectomy (Kitano and Kim, 1997).

80 A key challenge in liver surgery and especially in hepatectomy is to leave the patient with sufficient
81 functional capacity of the future remnant to survive and support liver regeneration while minimizing
82 complications. As a result, the decision whether or not a hepatectomy can be safely performed on a patient
83 is often based on predictions of postoperative remnant liver function (in addition to remnant liver volume),
84 which are in turn based on preoperative evaluations of liver function (and volume). Understanding how
85 cirrhosis alters liver function as measured via ICG is of high clinical relevance. Elucidating how ICG
86 parameters change with increasing CTP score would be an important asset for the evaluation of patients.

87 Important questions for the functional evaluation with ICG in the context of hepatectomy are (i) how
88 liver disease, especially cirrhosis, alter ICG elimination, and (ii) if postoperative survival can be predicted
89 from preoperative ICG measurements. Within this work a physiological-based computational model of
90 ICG pharmacokinetics was developed and applied to study these questions.

2 MATERIAL AND METHODS

91 2.1 Data

92 For the calibration and validation of the model a large data set of ICG measurements and physiological
93 data was established. All data is available via the pharmacokinetics database PK-DB ([https://pk-
94 db.com](https://pk-db.com)) (Grzegorzewski et al., 2021). PK-DB was used to encode the information on (i) patient
95 characteristics (e.g. age, disease, medication), (ii) applied interventions (e.g. ICG dosing, route of
96 application); (iii) measured ICG time-courses; and (iv) ICG pharmacokinetic parameters (e.g. ICG-PDR,
97 ICG-R15, ICG-clearance).

98 2.2 Indocyanine Green Pharmacokinetics Parameters

99 Pharmacokinetic parameters of ICG were calculated from the plasma-concentration time courses using
100 non-compartmental methods (Urso et al., 2002). The elimination rate constant (k_{el}) was calculated by fitting
101 the concentration-decay-curve to an exponential function: $c(t) = c(0) \cdot e^{-k_{el} \cdot t}$. ICG-PDR is k_{el} reported in
102 [%/min]. Half-life ($t_{1/2}$) was calculated as $\log(2)/k_{el}$. ICG-clearance was calculated as $CL = V_d \cdot k_{el}$, with
103 the apparent volume of distribution $V_d = D/(AUC_{\infty} \cdot k_{el})$. D is the applied dose of ICG and AUC_{∞} is
104 the area under the plasma-concentration time curve AUC calculated via the trapezoidal rule, extrapolated
105 until infinity. $ICG\text{-R15} = c(15)/c_{max}$ is calculated as the ratio between the plasma-concentration after 15
106 minutes and the maximum concentration c_{max} .

107 2.3 Model

108 The computational model is an ordinary differential equation (ODE) model encoded in the Systems
109 Biology Markup Language (SBML) (Hucka et al., 2019; Keating et al., 2020). It is defined as a set of
110 species (metabolites), compartments (organs and blood compartments) and reactions (processes such

111 as metabolic reactions and blood transport). The model was developed using sbmlutils (König, 2021b),
112 and cy3sbml (König and Rodriguez, 2019) and simulated using sbmlsim (König, 2021a) based on the
113 high-performance SBML simulator libroadrunner (Somogyi et al., 2015).

114 2.4 Model Parameterization

115 Values for organ volumes and tissue blood flows were taken from literature (ICRP, 2002). A subset
116 of model-parameters was determined using parameter-fitting to minimize the residuals between model
117 predictions and clinical data. This optimization-problem was solved using SciPy's least_squares method
118 and differential evolution algorithm (Virtanen et al., 2020). For the objective cost function F depending on
119 the parameters \vec{p} a simple L2-Norm was used consisting of the sum of weighted residuals

$$F(\vec{p}) = 0.5 \cdot \sum_{i,k} (w_k \cdot w_{i,k} \cdot r_{i,k}(\vec{p}))^2 = \sum_{i,k} (w_k \cdot w_{i,k} \cdot (y_{i,k} - m_{i,k}(\vec{p})))^2 \quad (1)$$

120 where $r_{i,k} = (y_{i,k} - m_{i,k}(\vec{p}))$ is the residual of time point i in time course k for model prediction $m_{i,k}(\vec{p})$
121 and the corresponding data point $y_{i,k}$; $w_{i,k}$ is the weighting of the respective data point i in timecourse
122 k based on the error of the data point and w_k = the weighting factor of time course k . Weighting of
123 time courses was based on the number of subjects per study. The final parameter set given in Tab. 2 was
124 determined using 250 runs of the local least square optimization (Fig. ??). The data used for the parameter
125 fit is listed in Tab. 1.

126 2.5 Uncertainty analysis

127 To evaluate the uncertainty of model predictions uncertainty analysis was performed for a subset of
128 simulations. Each model parameter was changed individually by $\pm 25\%$. From the set of resulting time
129 courses the mean, standard deviation (SD) and minimum and maximum values at each time point were
130 calculated. These uncertainty areas were displayed as shaded areas. Parameters corresponding to physical
131 constants (such as molecular weights) and dosing were not varied in the uncertainty analysis, as well as
132 parameters for conservation conditions such as the fractional blood flow through the lung (must be 1).

133 2.6 Classification

134 For the prediction of survival in hepatectomy multiple classification models were developed allowing
135 based on a set of features to predict the outcome after hepatectomy (binary classification: Survivors/Non-
136 Survivors). For model training and evaluation a dataset of 141 patients with information on survival status,
137 resection rate and preoperative ICG-R15 was used (Seyama and Kokudo, 2009; Wakabayashi et al., 2004).
138 Classification was performed using scikit-learn (Pedregosa et al., 2011) using a C-support vector classifier
139 with a polynomial kernel. Cross-validation was performed using the ShuffleSplit method with 200 iterations
140 and a train-test-ratio of 75%/25%. Based on the confusion matrix the following evaluation metrics were
141 calculated: precision, recall, balanced accuracy F1 score, Mathews correlation coefficient and receiver
142 operator curves (ROC).

3 RESULTS

143 Within this work a PBPK model of ICG pharmacokinetics was developed and applied to study (i) how liver
144 disease, especially cirrhosis, alter ICG elimination, and (ii) if postoperative survival can be predicted from
145 preoperative ICG measurements in the context of hepatectomy.

146 **3.1 Data**

147 A wide range of heterogeneous data was curated for model building (parameterization) and subsequent
148 model validation (comparison of model predictions to clinical data). An overview of the 29 studies with
149 their respective clinical protocols is provided in (Tab. 1). All data is freely available from <https://pk-db.com>.

150 **3.2 Model**

151 A PBPK model for the prediction of ICG pharmacokinetics was developed consisting of whole-body,
152 organ-level and hepatic metabolism. To simulate the whole-body distribution and hepatic elimination of
153 ICG two models were coupled: (i) A whole-body model (Fig. 1A) describing the distribution of ICG in the
154 body and to the organs via blood flow. (ii) A liver model (Fig. 1B) which describes hepatic uptake of ICG,
155 biliary excretion of ICG and transport of ICG into the feces. ICG specific pharmacokinetic parameters (i.e.
156 ICG-PDR, R15, clearance, half-life) were calculated from the resulting time course predictions of ICG in
157 venous plasma.

158 **3.2.1 Distribution and blood flow**

159 The distribution of ICG on whole-body level is modeled using a network of blood flows representing
160 the systemic circulation. From the venous blood, ICG is transported through the lung into the arterial
161 blood from where it can reach the liver on two paths: (i) through the hepatic artery and (ii) through the
162 gastrointestinal tract reaching the liver via the portal vein. Because the liver is the only tissue partaking in
163 the uptake and elimination of ICG, all other organs (e.g. kidney, heart, adipose tissue, muscle, etc.) were
164 pooled into the rest compartment. Each organ consists of a blood compartment (representing the vessels)
165 and a tissue compartment. ICG transport via blood flow was implemented as irreversible transport. The
166 transport v_i from compartment i to the next compartment is determined by the ICG concentration C_i in
167 compartment i and a compartment-specific blood flow Q_i . Q_i is determined by the cardiac output Q_{CO}
168 and a compartment specific fractional tissue blood flow fQ_i . Multiple conservation conditions hold in
169 the model to ensure mass and flow balance. First the sum of blood flows from the arterial to the venous
170 compartment must equal the sum of flows in the reverse direction: $Q_{CO} = Q_{lu} = Q_h + Q_{re}$. Flow into an
171 organ must be equal to the flow out of the organ. E.g. hepatic venous blood flow must be equal to the sum
172 of hepatic arterial and portal venous blood flow: $Q_h = Q_{ha} + Q_{po}$.

173 **3.2.2 Hepatic metabolism and biliary excretion**

174 The liver model (Fig. 1B) consists of three consecutive transport reactions of ICG. After ICG is taken
175 up in the liver it is excreted into the bile. Both transport reactions are modeled as irreversible Michaelis-
176 Menten-kinetics. From the bile, ICG is transported into the feces modeled via a first order kinetic. All
177 transport kinetics scale with the liver volume V_{li} .

178 **3.2.3 Parameter fitting**

179 Parameter fitting of the model was performed using a subset of ICG time courses and extraction-ratio
180 measurements (see Tab. 1). No ICG pharmacokinetic parameters were used in model fitting. Overall, 5
181 model parameters were fitted (see Tab. 2). Two of them determine the import of ICG in the liver, three
182 determine the subsequent excretion in the bile. The agreement between fit data and model predictions
183 improved substantially during parameter fitting and all trainings data with the exception of three simulations
184 (Meijer1988, Chijiwa2000 and Burns1991) could be described very well after parameter fitting.

185 **3.2.4 Modeling liver cirrhosis**

186 The reference model, representing a healthy human subject, was adjusted to simulate cirrhosis by
187 including a combination of functional tissue loss (due to scarring and necrosis in cirrhosis) and the
188 formation of intrahepatic shunts, both key hallmarks of cirrhosis (Fig. 1C). The loss of functional liver
189 tissue was controlled via the parameter $f_{tissue_loss} \in [0, 1]$ which defines the fraction of parenchymal

190 cell volume lost in the liver due to the disease. For modeling arteriohepatic and portosystemic shunts two
191 additional blood vessels were introduced into the model. They connect the hepatic artery and the portal
192 vein directly to the hepatic vein. As a result, a part of the portal venous and arterial blood bypasses the
193 active liver tissue and is shunted to the hepatic venous blood compartment, so that ICG can not be extracted
194 (corresponding to *in silico* shunts). The amount of blood that flows through the shunts is determined by the
195 parameter $f_{shunts} \in [0, 1]$, which defines the fraction of blood bypassing the liver. The remaining blood
196 $(1 - f_{shunts})$ reaches the liver tissue and ICG can be extracted. To simulate various degrees of cirrhosis the
197 parameters f_{shunts} and f_{tissue_loss} were varied in lockstep by coupling them into the parameter $f_{cirrhosis}$.
198 The following values for $f_{cirrhosis}$ were used: healthy - 0.0, mild cirrhosis - 0.38, moderate cirrhosis - 0.69,
199 severe cirrhosis - 0.81.

200 **3.2.5 Modeling hepatectomy**

201 The developed model allows to predict changes in ICG pharmacokinetic parameters after hepatectomy
202 (Fig. 1D). *In silico* hepatectomies were simulated by reducing the fractional liver volume $FVli$ by up to
203 90% (corresponding to a resection rate of 90%). The absolute liver volume is determined with the body
204 weight BW via $FVli \cdot BW$. All hepatectomies were simulated under varying degrees of cirrhosis as
205 described above.

206 **3.3 Healthy controls**

207 In a first step the fitted model was evaluated with the data used for model calibration consisting of ICG
208 time courses in healthy subjects (Fig. 2). For the simulations infusion protocols and body weights were
209 adjusted as reported in the respective studies (see Tab. 1 for details). If no body weight was reported 75 kg
210 were assumed.

211 The model predictions for ICG plasma disappearance curves after an ICG bolus are in good agreement
212 with the clinical data (Andersen et al., 1999; Grundmann et al., 1992; Kamimori et al., 2000; Klockowski
213 et al., 1990; Niemann et al., 2000; Meijer et al., 1988). In addition, more complex infusion protocols as
214 reported in Soons et al. (Soons et al., 1991) can also be described (Fig. 2F), infusion protocol of three
215 different infusion rates ($2.0 \rightarrow 0.5 \rightarrow 1.0$ mg/min, each for 40 minutes). Due to the high extraction-ratio of
216 ICG by the liver, the plasma concentration reaches steady state quickly after each change in the infusion
217 rate. Next, simulations of the biliary excretion rate of ICG after bolus administrations of 0.5, 1.0 and 2.0
218 mg/kg ICG were performed and the results were compared to clinical data (Meijer et al., 1988; Chijiwa
219 et al., 2000).

220 Finally, simulations of constant infusions were performed and compared to reported arterial and hepatic
221 vein time courses of ICG (Leevy et al., 1962) and ICG extraction ratios (Leevy et al., 1962; Grainger et al.,
222 1983).

223 Overall, the model shows the ability to accurately predict ICG time courses for venous and arterial
224 plasma concentrations, for hepatic vein concentrations, the biliary excretion rate and extraction ratios when
225 compared to clinical data. Especially plasma time courses of ICG after ICG bolus and ICG infusion are
226 very well predicted by the model, even for varying administration protocols (dosing and infusion rates).

227 In a next step a systematic analysis of the dose dependency of ICG pharmacokinetic parameters was
228 performed (Fig. 3). A dose-dependency of the ICG parameters can only be observed if the ICG dose
229 exceeds 100 mg (much higher than the typically applied doses of 20 - 35 mg), resulting in a reduction in
230 ICG-clearance and ICG-PDR as well as an increase of ICG-R15 and ICG-t_{1/2} (Fig. 3A-D). The model
231 predictions could be validated with clinical data (Martin et al., 1975, 1976; Meijer et al., 1988) (Fig. 3E-G).

232 **3.4 Cirrhosis**

233 To simulate changes of ICG pharmacokinetics in cirrhosis, hepatic tissue loss and shunts were included
234 in the model as described above. First, a systematic analysis of the effect of intrahepatic shunts (f_{shunts}),
235 functional tissue loss (f_{tissue_loss}) and the combination of both ($f_{cirrhosis}$) on ICG pharmacokinetic
236 parameters was performed (Fig. 4A-D). All three parameters were varied from 0 (no effect, healthy control)
237 to 0.9 (severe effect). ICG-clearance and ICG-PDR decrease with increasing $f_{cirrhosis}$ whereas ICG-R15
238 and ICG-t_{1/2} increase. The loss of a fraction of functional liver tissue appears to have a smaller effect on
239 ICG pharmacokinetic parameters than shunting of an equal fraction of blood past the liver. When f_{shunts}
240 and f_{tissue_loss} are combined to $f_{cirrhosis}$ their effect on ICG pharmacokinetic parameters is additive. For
241 ICG-clearance and ICG-PDR the effects of both parameters combine to an almost linear dependency on
242 $f_{cirrhosis}$. The decrease in ICG-clearance and ICG-PDR with increasing cirrhosis and increase of ICG-R15
243 and ICG-t_{1/2} with increasing cirrhosis can be observed over a wide range of applied ICG doses (Fig. 3A-D).

244 By varying the $f_{cirrhosis}$ parameter from 0 to 0.9 different degrees of cirrhosis were simulated and the
245 nonlinear relation between ICG-R20 and ICG-kel as well as ICG-R20 and ICG-t_{1/2} could be predicted
246 (Fig. 4E,F). As seen in the systematic analysis (Fig. 4A-D) ICG-t_{1/2} and ICG-R20 increase with cirrhosis
247 whereas ICG-kel decreases. The correlation between the ICG pharmacokinetic parameters is predicted
248 accurately by the model when compared to a clinical dataset that lacks information about the severity of
249 liver cirrhosis of its patients (Cherrick et al., 1960; Caesar et al., 1961). Next the ICG-PDR in cirrhotic
250 patients, acute and recovering hepatitis and control subjects after different doses of ICG (0.5 mg/kg and 5.0
251 mg/kg ICG) was compared to the model predictions. The clinical data shows higher ICG-PDR values after
252 an ICG dose of 0.5 mg/kg than after an ICG dose of 5.0 mg/kg (Levy et al., 1967). In the model prediction
253 the ICG-PDR in acute and recovering hepatitis resembles that of mild to moderate cirrhosis (Fig. 4G).
254 ICG-clearances after a bolus administration and during a constant infusion show good positive correlation
255 in cirrhotic patients (Burns et al., 1991). This correlation is predicted accurately by the model (Fig. 4H).

256 Having evaluated and validated the effect of $f_{cirrhosis}$ on the model prediction of ICG parameters, we
257 were interested how the model $f_{cirrhosis}$ parameter compares to the *in vivo* estimation of cirrhosis degree
258 via the CTP-score (Fig. 5). As described above, the CTP-score is a semi-quantitative scoring system
259 that describes the severity of liver cirrhosis. An important step to apply the developed PBPK model in a
260 clinical setting, is the ability to adjust the model individually to the respective status of liver disease in
261 a patient. Therefore, the relationship between the $f_{cirrhosis}$ parameter and the CTP-Score was evaluated
262 using multiple datasets in which ICG pharmacokinetic parameters were reported in patient subgroups of
263 different CTP-Scores (Figg et al., 1995; Møller et al., 1998, 2019; Herold et al., 2001).

264 The clinical results of the ICG pharmacokinetic parameters in different CTP-classes were mapped onto
265 their respective systematic scan (Fig. 5A-D). The resulting $f_{cirrhosis}$ values were then compared between
266 the patient groups. Additional individual data is shown (Figg et al., 1995).

267 The resulting mapping between $f_{cirrhosis}$ and the CTP-classes shows a good positive correlation. The
268 $f_{cirrhosis}$ values for the controls groups are close to 0, increasing with the CTP-class. The relation appears
269 nonlinear, as $f_{cirrhosis}$ shows little difference between CTP-class B and C. The mappings of the CTP-class
270 to $f_{cirrhosis}$ for the different ICG parameters each give very similar results. From the mapping of all
271 four pharmacokinetic parameters a mean value of $f_{cirrhosis}$ was calculated for each CTP-class (Control:
272 $f_{cirrhosis} = 0.0$; Mild cirrhosis: 0.38; Moderate cirrhosis: 0.69; Severe cirrhosis: 0.81). The resulting
273 values were used in all simulations of control, mild, moderate and severe cirrhosis, as well as in the above
274 described dose dependency analysis (Fig. 3A-D).

275 Only a single study reported the numerical CTP-score of the patient groups in combination with ICG-
276 clearance (Figg et al., 1995). All other studies instead used the CTP-classes (A, B, C) (Møller et al., 1998,
277 2019; Herold et al., 2001). With a dataset of individually reported CTP-scores in combination with ICG
278 pharmacokinetic parameters of cirrhotic patients, it would be possible to calculate the relationship of the
279 CTP-score on the $f_{cirrhosis}$ parameter more accurately. Such an improved mapping would allow to adjust
280 the model via the $f_{cirrhosis}$ parameter individually based on the respective severity of liver disease/cirrhosis
281 of the patient reported as CTP-score.

282 After establishing the CTP mapping the model was further validated via several comparisons with clinical
283 data of ICG time courses in cirrhotic and control subjects (Fig. 6).

284 Assuming moderate cirrhosis ($f_{cirrhosis} = 0.7$), the model prediction of an ICG time course in a cirrhotic
285 patient agrees well with the clinical data (Burns et al., 1991) (Fig. 6A,B). The main alteration compared
286 to the healthy control is the slower disappearance rate resulting in higher ICG plasma concentrations.
287 The same effect is observed in steady state via a constant ICG infusion (Fig. 6C). Using the $f_{cirrhosis}$
288 values from the CTP mapping above, the steady state concentrations are predicted in agreement with the
289 clinical data (Caesar et al., 1961). Fig. 6D,E shows the relation between the hepatic venous and arterial ICG
290 concentrations and the extraction ratio in a cirrhotic subject. Here, $f_{cirrhosis}$ was set to 0.54 which allowed
291 to predict arterial and hepatic vein concentration as well as ICG extraction ratio. Finally, in Fig. 6F-H the
292 ICG extraction ratio predicted for controls and three different cirrhosis degrees was compared to clinical
293 data (Levy et al., 1962; Gadano et al., 1997; Caesar et al., 1961). The extraction ratio in cirrhotic subjects
294 is reduced compared to healthy controls, as predicted by the model.

295 3.5 Hepatectomy

296 After validating the model predictions of ICG pharmacokinetics in liver cirrhosis, the model was applied
297 to liver surgery, specifically hepatectomy. To analyze the effect of hepatectomy on ICG elimination the
298 change in ICG pharmacokinetic parameters as a function of the resection rate was simulated (Fig. 7A-D).
299 The scan was performed for healthy controls as well as three different degrees of cirrhosis.

300 ICG-clearance and ICG-PDR are highest in the preoperative liver (resection rate = 0) and decrease with
301 increasing resection rate whereas ICG-t_{1/2} and ICG-R15 are lowest in the healthy liver and increase with
302 increasing resection rate. The effect of varying the degree of cirrhosis is in accordance with the results
303 shown in (Fig. 4A-D). Importantly, increasing resection rate and increasing degree of cirrhosis affect
304 ICG pharmacokinetic parameters in the same manner. The dependencies of ICG-clearance, ICG-PDR,
305 ICG-t_{1/2} and ICG-R15 on the resection rate are fairly linear up to 50-60% resection, and become much
306 more non-linear for higher resection rates.

307 For model validation the predictions were compared to clinical data of subjects undergoing hepatectomy.
308 For these simulations the resection rate was varied from 0 to 0.9. First, the relative change of ICG-PDR after
309 hepatectomy as a function of the resection rate was simulated (Fig. 7E). The model predicts a nonlinear
310 dependency of change in ICG-PDR on the change of liver volume independent of the degree of cirrhosis.
311 This prediction is in good agreement with the clinical data (Thomas et al., 2015; Stockmann et al., 2009).
312 Furthermore, the correlation between measured postoperative ICG-kel and estimated remnant ICG-kel
313 (ICG-kel · fractional liver remnant) was simulated under various degrees of cirrhosis (Fig. 7F). A good
314 correlation can be observed. The model predictions were compared to three different data sets (Ohwada
315 et al., 2006; Okochi et al., 2002; Sunagawa et al., 2021) and are in good agreement with them. In addition,
316 all data sets are in good agreement with each other. The simulated correlation line is independent of the
317 cirrhosis degree, but with increasing cirrhosis ICG-kel decreases. A large variability can be observed in the

318 experimental data, but as our simulations indicate is most likely not due to the underlying liver disease
319 (cirrhosis).

320 (Thomas et al., 2015) found significant correlation between post-hepatectomy ICG-PDR and
321 intraoperative ICG-PDR measured under trial clamping of those parts of the liver that were to be removed.
322 This was simulated by changing hepatic blood flow and liver volume in separate simulations but in the same
323 intervals. This was performed for a healthy liver as well as three different degrees of cirrhosis (Fig. 7G).
324 The predictions agree well with the clinical data and show that reducing hepatic blood flow (clamping of
325 liver volumes which will be resected) has a very similar effect on ICG elimination as actually removing the
326 respective liver volume via hepatectomy.

327 Finally, the correlation between preoperative and postoperative ICG-PDR for different resection rates and
328 cirrhosis degrees was simulated and compared to clinical data (Fig. 7H). ICG-PDR is reduced in cirrhosis
329 preoperatively as well as postoperatively. The model prediction agrees with the clinical data (Thomas et al.,
330 2015).

331 Overall the predictions of hepatectomies in severely cirrhotic liver is not in good agreement with the
332 clinical data. This reflects the fact that no resections are performed in severely cirrhotic liver due to high
333 risk of postoperative complications. As a consequence, most of the hepatectomies are performed in mild
334 to moderate cirrhosis. The model allows to perform these risky hepatectomies *in silico* and predict their
335 effect.

336 In summary, the model allows to systematically predict the changes of ICG pharmacokinetic parameters
337 in hepatectomy under various degrees of liver disease (cirrhosis).

338 **3.6 Prediction of post-hepatectomy survival**

339 An interesting application of the presented PBPK model is the prediction of postoperative outcome for
340 patients undergoing hepatectomy. Preoperative ICG-R15 and the planned resection rate are key parameters
341 included in the decision process whether a patient is eligible to receive liver resection surgery.

342 As shown above, the presented PBPK model accurately predicts ICG-R15 in liver cirrhosis as well as the
343 changes in ICG-R15 following hepatectomy. As such, we were interested how a classification model based
344 on the PBPK model prediction of postoperative ICG-R15 compares to classification approaches only using
345 clinical data (preoperative ICG-R15, resection rate and calculated postoperative ICG-R15).

346 Five different classification models to predict survival after hepatectomy were developed using a dataset
347 of 141 patients (Seyama and Kokudo, 2009; Wakabayashi et al., 2004): Three data-based classification
348 models based on (i) the preoperative ICG-R15 (Data1A), (ii) the calculated postoperative ICG-R15 by
349 multiplying the future liver remnant (1-resection rate) and preoperative ICG-R15 (Data1B) and (iii) both the
350 resection rate and the preoperative ICG-R15 (Data2). In addition two PBPK-based models were developed,
351 (iv) one based on the prediction of postoperative ICG-R15 (PBPK1) and (v) the other based on the resection
352 rate and the estimated $f_{cirrhosis}$ model parameter (PBPK2). By fitting the model parameter $f_{cirrhosis}$ as a
353 function of its resulting ICG-R15 value to a logarithmic function $f_{cirrhosis} = a \cdot \ln(b \cdot x) + c$ where x is
354 the ICG-R15 value, the clinically measured preoperative ICG-R15 value could be converted to a value of
355 the model parameter $f_{cirrhosis}$, thereby providing an estimate of individual liver disease (cirrhosis degree).
356 This estimated parameter allowed in combination with the resection rate to predict individual postoperative
357 ICG-R15 values. An overview of the classification results of these five models is provided in Tab. 3.

358 A clear difference in the ability to predict survival after hepatectomy exists between the single feature
359 data-based classifiers (Data1A, Data1B) and the other classifiers. Both PBPK-based classifiers (PBPK1,

360 PBPK2) as well as the Data2 classifier outperform the Data1A and Data1B classifiers. When comparing
361 the classification models using a single feature (Data1A, Data1B, PBPK1) the physiological-based
362 predicted postoperative ICG-R15 (PBPK1) clearly outperforms the preoperative (Data1A) and calculated
363 postoperative ICG-R15 (Data1B).

364 Fig. 8A shows the postoperative ICG-R15 in survivors and non-survivors predicted by the model as well
365 as the preoperative ICG-R15 in the same subjects (inlet). The predicted postoperative ICG-R15 is able to
366 distinguish better between survivors and non-survivors than the preoperative ICG-R15 as can be seen by
367 the clearer separation of the histograms and the ROC curves for the single feature classifier (Fig. 8C). Both
368 preoperative ICG-R15 as well as calculated postoperative ICG-R15 are not very useful for the prediction of
369 survival after hepatectomy, whereas predicted postoperative ICG-R15 using PBPK1 is a very good measure
370 for survival.

371 To determine possible cutoffs for predicted postoperative ICG-R15 based on the PBPK1 classifier the
372 dependency of evaluation metrics on the cutoff was analyzed (Fig. 8B). Balanced accuracy has a maximum
373 at around 40%, precision would be perfect for a predicted ICG-R15 ; 20%. Fig. 8D depicts how the
374 predicted postoperative ICG-R15 depends on the resection rate and $f_{cirrhosis}$. The data confirms that a
375 cutoff value slightly below 40% would correctly predict most of the non-survivors with a stricter cutoff of
376 20% avoiding any death after hepatectomy. Similar analysis of the data-based single feature classification
377 models failed to find a significant optimum of evaluation metrics for either preoperative ICG-R15 or
378 calculated postoperative ICG-R15 (Fig. 9).

379 The two-feature classification models (PBPK2, Data2) show good performance in the survival prediction
380 comparable to PBPK1 as can be seen from the ROC-curves in Fig. 8F. Whereas the one-dimensional
381 PBPK1 classifier provides a simple interpretation and cutoff value, the two dimensional classifiers are more
382 difficult to interpret and apply.

383 In summary, we developed a single-feature classification model based on a physiological-based model of
384 ICG elimination (PBPK1) which allows to predict post-hepatectomy survival solely based on preoperative
385 ICG-R15 input. Importantly, this computational model-based approach clearly outperforms data-based
386 approaches such as preoperative ICG-R15 and calculated postoperative ICG-R15.

4 DISCUSSION

387 In summary, a PBPK model for ICG based liver function evaluation was developed, validated, and applied to
388 the prediction of postoperative outcome after liver surgery, i.e., survival after hepatectomy. The model takes
389 into account physiological factors such as the degree of cirrhosis and the planned resection volume, which
390 allowed an accurate prediction of postoperative liver function in agreement with clinical data. As such, the
391 model has proven its potential of becoming a valuable clinical tool for the planning of hepatectomies.

392 The physiologically-based modeling approach allowed us to predict ICG pharmacokinetics data from
393 29 studies using only a small set of parameters and processes. The model accurately predicts changes in
394 ICG pharmacokinetic parameters in a wide range of conditions including varying degrees of cirrhosis.
395 Additionally, *in silico* hepatectomies with underlying cirrhosis are in good agreement with clinical data. As
396 an important note, all clinical data besides the time courses in healthy subjects used for model calibration
397 was used for model validation.

398 An important outcome of this study is a single-feature classification model based on a physiological-based
399 model of ICG elimination (PBPK1) which allows to predict post-hepatectomy survival solely based on
400 preoperative ICG-R15 and resection rate. A limitation hereby is the relative small sample size (n=104)

401 from retrospective data. Validation with a dataset consisting of Caucasian subjects would be highly relevant,
402 as the available survival data after hepatectomy was based on Japanese subjects.

403 The developed classification models show the potential of using PBPK predicted postoperative ICG-R15
404 values in the clinical decision process. Whereas the PBPK1 classifier provides a simple cutoff based on
405 the individual model prediction (Fig. 8AB), PBPK2 provides the dependency of predicted postoperative
406 ICG-R15 on resection rate and cirrhosis degree (Fig. 8D), both key factors for survival after hepatectomy.
407 Comparing different approaches of predicting postoperative outcome after hepatectomy showed the
408 importance of taking resection rate into account. The data-based classifier combining resection rate with
409 preoperative ICG (Data2) allowed to achieve comparable classification results than the PBPK-based
410 classifiers. In contrast, the classification models Data1A and Data1B failed to achieve satisfying results, i.e.
411 neither preoperative ICG alone nor calculated postoperative ICG provide sufficient information.

412 Due to the high mortality rate major hepatectomy in the presence of cirrhosis is considered to be
413 contraindicated. Recommendations are often that only selected patients with Child's A status or ICG-R15
414 of less than 10% undergo major hepatectomy (Kitano and Kim, 1997). As can be seen in Fig. 8A inlet even
415 such a strict cutoff can still result mortality after hepatectomy. A better approach is to use a combination of
416 resection rate and individual cirrhosis degree as shown by the PBPK2 classifier (and indirect by the PBPK1
417 classifier).

418 Overall, the clinical data shows large variability in ICG pharmacokinetic measurements, mostly due
419 to intra-individual differences (e.g. Fig. 7F). Possible explanations are differences in blood flow, plasma
420 proteins or protein amount or activity of the ICG transporters. An important next step would be a systematic
421 analysis of these possible causes of variability and account for these confounding factors.

422 Importantly, due the physiological-based modeling approach predictions could be easily further
423 individualized with the availability of respective data. The individualization of the model could include
424 general information such as age, sex and ethnicity. Physiological information such as body weight,
425 body fat percentage, cardiovascular parameters and organ volumes would be included. Information
426 regarding the liver specifically would be of high relevance. This includes liver perfusion, liver volume and
427 quantification of ICG protein amounts as well as assessment of liver disease such as cirrhosis degree. Such
428 an individualization could substantially improve the models prediction of postoperative liver function and
429 outcome in patients undergoing hepatectomy.

430 Going forward, an important step will be to evaluate the model in the clinical context using a high quality
431 dataset reporting individual ICG time courses in combination with the above-mentioned additional clinical
432 data.

CONFLICT OF INTEREST STATEMENT

433 All authors declare that the research was conducted in the absence of any commercial or financial
434 relationships that could be construed as a potential conflict of interest.

AUTHOR CONTRIBUTIONS

435 AK and MK designed the study, developed the computational model, build the classifiers, performed the
436 analysis, and wrote the initial draft of the manuscript. JG provided support with PKDB, data curation
437 and meta-analysis. AK and MK wrote the initial manuscript draft. All authors contributed and revised the
438 manuscript critically.

FUNDING

439 MK is supported by the Federal Ministry of Education and Research (BMBF, Germany) within the
440 research network Systems Medicine of the Liver (LiSyM, grant number 031L0054). This work was
441 supported by the German Research Foundation (DFG) within the Research Unit Programme FOR 5151
442 "QuaLiPerF (Quantifying Liver Perfusion-Function Relationship in Complex Resection - A Systems
443 Medicine Approach)" by grant number 436883643.

SUPPLEMENTAL DATA

444 Supplementary Material should be uploaded separately on submission, if there are Supplementary Figures,
445 please include the caption in the same file as the figure. LaTeX Supplementary Material templates can be
446 found in the Frontiers LaTeX folder.

DATA AVAILABILITY STATEMENT

447 The datasets generated for this study can be found in PK-DB available from <https://pk-db.com>.

REFERENCES

- 448 Andersen, V., Sonne, J., and Larsen, S. (1999). Antipyrine, oxazepam, and indocyanine green clearance in
449 patients with chronic pancreatitis and healthy subjects. *Scandinavian journal of gastroenterology* 34,
450 813–817. doi:10.1080/003655299750025750
- 451 Bernstein, L. M., Wheeler, J. X., E E, B. O. N. D., Rohmsdahl, M., and Dougherty, N. (1960). The blood
452 galactose disappearance curve as a test of liver function. *Gastroenterology* 39, 293–304
- 453 Botero, R. C. and Lucey, M. R. (2003). Organ allocation: model for end-stage liver disease, child-
454 turcotte-pugh, mayo risk score, or something else. *Clinics in liver disease* 7, 715–27, ix. doi:10.1016/
455 s1089-3261(03)00052-7
- 456 Burns, E., Triger, D. R., Tucker, G. T., and Bax, N. D. (1991). Indocyanine green elimination in patients
457 with liver disease and in normal subjects. *Clinical science (London, England : 1979)* 80, 155–160
- 458 Caesar, J., Shaldon, S., Chiandussi, L., Guevara, L., and Sherlock, S. (1961). The use of indocyanine green
459 in the measurement of hepatic blood flow and as a test of hepatic function. *Clinical science* 21, 43–57
- 460 Cherrick, G. R., Stein, S. W., Leevy, C. M., and Davidson, C. S. (1960). Indocyanine green: observations
461 on its physical properties, plasma decay, and hepatic extraction. *The Journal of clinical investigation* 39,
462 592–600. doi:10.1172/JCI104072
- 463 Chijiwa, K., Watanabe, M., Nakano, K., Noshiro, H., and Tanaka, M. (2000). Biliary indocyanine green
464 excretion as a predictor of hepatic adenosine triphosphate levels in patients with obstructive jaundice.
465 *American journal of surgery* 179, 161–166. doi:10.1016/s0002-9610(00)00274-9
- 466 Child, C. G. and Turcotte, J. G. (1964). Surgery and portal hypertension. *Major problems in clinical
467 surgery* 1, 1–85
- 468 Figg, W. D., Dukes, G. E., Lesesne, H. R., Carson, S. W., Songer, S. S., Pritchard, J. F., et al. (1995).
469 Comparison of quantitative methods to assess hepatic function: Pugh's classification, indocyanine green,
470 antipyrine, and dextromethorphan. *Pharmacotherapy* 15, 693–700
- 471 Filmann, N., Walter, D., Schadde, E., Bruns, C., Keck, T., Lang, H., et al. (2019). Mortality after liver
472 surgery in germany. *The British journal of surgery* 106, 1523–1529. doi:10.1002/bjs.11236
- 473 Gadano, A., Hadengue, A., Vachiery, F., Moreau, R., Sogni, P., Soupison, T., et al. (1997). Relationship
474 between hepatic blood flow, liver tests, haemodynamic values and clinical characteristics in patients
475 with chronic liver disease. *Journal of gastroenterology and hepatology* 12, 167–171. doi:10.1111/j.
476 1440-1746.1997.tb00401.x

- 477 Gilmore, I. T., Marigold, J. H., and Thompson, R. P. (1982). Half-life time or clearance of indocyanine
478 green in patients with liver disease. *Hepato-gastroenterology* 29, 55–57
- 479 Gorowska-Kowolik, K., Chobot, A., and Kwiecien, J. (2017). javax.xml.bind.jaxbelement@77416ce1, c
480 methacetin breath test for assessment of microsomal liver function: Methodology and clinical application.
481 *Gastroenterology research and practice* 2017, 7397840. doi:10.1155/2017/7397840
- 482 Grainger, S. L., Keeling, P. W., Brown, I. M., Marigold, J. H., and Thompson, R. P. (1983). Clearance and
483 non-invasive determination of the hepatic extraction of indocyanine green in baboons and man. *Clinical
484 science (London, England : 1979)* 64, 207–212
- 485 Grundmann, U., Ziehmer, M., Raahimi, H., Altmayer, P., Larsen, R., and Büch, H. P. (1992). [effect of the
486 volatile anesthetics halothane, enflurane and isoflurane on liver circulation in the human]. *Anasthesiologie,
487 Intensivmedizin, Notfallmedizin, Schmerztherapie : AINS* 27, 406–413. doi:10.1055/s-2007-1000324
- 488 Grzegorzewski, J., Brandhorst, J., Green, K., Eleftheriadou, D., Dupont, Y., Barthorscht, F., et al. (2021).
489 Pk-db: pharmacokinetics database for individualized and stratified computational modeling. *Nucleic
490 acids research* 49, D1358–D1364. doi:10.1093/nar/gkaa990
- 491 Hackl, C., Schlitt, H. J., Renner, P., and Lang, S. A. (2016). Liver surgery in cirrhosis and portal
492 hypertension. *World journal of gastroenterology* 22, 2725–2735. doi:10.3748/wjg.v22.i9.2725
- 493 Herold, C., Heinz, R., Radespiel-Tröger, M., Schneider, H. T., Schuppan, D., and Hahn, E. G. (2001).
494 Quantitative testing of liver function in patients with cirrhosis due to chronic hepatitis c to assess disease
495 severity. *Liver* 21, 26–30. doi:10.1034/j.1600-0676.2001.210104.x
- 496 Hucka, M., Bergmann, F. T., Chaouiya, C., Dräger, A., Hoops, S., Keating, S. M., et al. (2019). The
497 systems biology markup language (sbml): Language specification for level 3 version 2 core release 2.
498 *Journal of Integrative Bioinformatics*
- 499 ICRP (2002). Basic anatomical and physiological data for use in radiological protection: reference values.
500 a report of age- and gender-related differences in the anatomical and physiological characteristics of
501 reference individuals. icrp publication 89. *Annals of the ICRP* 32, 5–265
- 502 Jin, S., Fu, Q., Wuyun, G., and Wuyun, T. (2013). Management of post-hepatectomy complications. *World
503 journal of gastroenterology* 19, 7983–7991. doi:10.3748/wjg.v19.i44.7983
- 504 Kamimori, G. H., Sirisuth, N., Greenblatt, D. J., and Eddington, N. D. (2000). The influence of the
505 menstrual cycle on triazolam and indocyanine green pharmacokinetics. *Journal of clinical pharmacology*
506 40, 739–744. doi:10.1177/00912700022009495
- 507 Keating, S. M., Waltemath, D., König, M., Zhang, F., Dräger, A., Chaouiya, C., et al. (2020). Sbml level 3:
508 an extensible format for the exchange and reuse of biological models. *Molecular systems biology* 16,
509 e9110. doi:10.15252/msb.20199110
- 510 Keiding, S., Ott, P., and Bass, L. (1993). Enhancement of unbound clearance of icg by plasma proteins,
511 demonstrated in human subjects and interpreted without assumption of facilitating structures. *Journal of
512 hepatology* 19, 327–344
- 513 Kitano, S. and Kim, Y. I. (1997). Icg clearance in assessing cirrhotic patients with hepatocellular carcinoma
514 for major hepatic resection. *HPB surgery : a world journal of hepatic, pancreatic and biliary surgery* 10,
515 182–183. doi:10.1155/1997/69231
- 516 Klockowski, P. M., Lener, M. E., Sirgo, M. A., and Rocci, M. L. (1990). Comparative evaluation of the
517 effects of isradipine and diltiazem on antipyrine and indocyanine green clearances in elderly volunteers.
518 *Clinical pharmacology and therapeutics* 48, 375–380. doi:10.1038/clpt.1990.165
- 519 [Dataset] König, M. (2021a). matthiaskoenig/sbmlsim: 0.1.14 - sbml simulation made easy. doi:10.5281/
520 zenodo.4569155

- 521 [Dataset] König, M. (2021b). matthiaskoenig/sbmlutils: 0.4.12 - python utilities for sbml. doi:10.5281/
522 zenodo.4595467
- 523 [Dataset] König, M. and Rodriguez, N. (2019). matthiaskoenig/cy3sbml: cy3sbml-v0.3.0 - SBML for
524 Cytoscape. doi:10.5281/zenodo.3451319
- 525 Leevy, C. M., Mendenhall, C. L., Lesko, W., and Howard, M. M. (1962). Estimation of hepatic blood flow
526 with indocyanine green. *The Journal of clinical investigation* 41, 1169–1179. doi:10.1172/JCI104570
- 527 Leevy, C. M., Smith, F., Longueville, J., Paumgartner, G., and Howard, M. M. (1967). Indocyanine green
528 clearance as a test for hepatic function. evaluation by dichromatic ear densitometry. *JAMA* 200, 236–240
- 529 Martin, J. F., Mikulecky, M., Blaschke, T. F., Waggoner, J. G., Vergalla, J., and Berk, P. D. (1975).
530 Differences between the plasma indocyanine green disappearance rates of normal men and women.
531 *Proceedings of the Society for Experimental Biology and Medicine. Society for Experimental Biology*
532 and *Medicine (New York, N.Y.)* 150, 612–617
- 533 Martin, J. F., Vierling, J. M., Wolkoff, A. W., Scharschmidt, B. F., Vergalla, J., Waggoner, J. G., et al.
534 (1976). Abnormal hepatic transport of indocyanine green in gilbert's syndrome. *Gastroenterology* 70,
535 385–391
- 536 Meijer, D. K., Weert, B., and Vermeer, G. A. (1988). Pharmacokinetics of biliary excretion in man. vi.
537 indocyanine green. *European journal of clinical pharmacology* 35, 295–303
- 538 Mukherjee, S., Rogers, M. A. M., and Buniak, B. (2006). Comparison of indocyanine green clearance with
539 child's-pugh score and hepatic histology: a multivariate analysis. *Hepato-gastroenterology* 53, 120–123
- 540 Møller, S., Hillingsø, J., Christensen, E., and Henriksen, J. H. (1998). Arterial hypoxaemia in cirrhosis:
541 fact or fiction? *Gut* 42, 868–874. doi:10.1136/gut.42.6.868
- 542 Møller, S., la Cour Sibbesen, E., Madsen, J. L., and Bendtsen, F. (2019). Indocyanine green retention
543 test in cirrhosis and portal hypertension: Accuracy and relation to severity of disease. *Journal of*
544 *gastroenterology and hepatology* 34, 1093–1099. doi:10.1111/jgh.14470
- 545 Niemann, C. U., Henthorn, T. K., Krejcie, T. C., Shanks, C. A., Enders-Klein, C., and Avram, M. J.
546 (2000). Indocyanine green kinetics characterize blood volume and flow distribution and their alteration
547 by propranolol. *Clinical pharmacology and therapeutics* 67, 342–350. doi:10.1067/mcp.2000.104945
- 548 Ohwada, S., Kawate, S., Hamada, K., Yamada, T., Sunose, Y., Tsutsumi, H., et al. (2006). Perioperative
549 real-time monitoring of indocyanine green clearance by pulse spectrophotometry predicts remnant liver
550 functional reserve in resection of hepatocellular carcinoma. *The British journal of surgery* 93, 339–346.
551 doi:10.1002/bjs.5258
- 552 Okochi, O., Kaneko, T., Sugimoto, H., Inoue, S., Takeda, S., and Nakao, A. (2002). Icg pulse
553 spectrophotometry for perioperative liver function in hepatectomy. *The Journal of surgical research* 103,
554 109–113. doi:10.1006/jsre.2001.6328
- 555 Pedregosa, F., Varoquaux, G., Gramfort, A., Michel, V., Thirion, B., Grisel, O., et al. (2011). Scikit-learn:
556 Machine learning in Python. *Journal of Machine Learning Research* 12, 2825–2830
- 557 Pind, M.-L. L., Bendtsen, F., Kallemose, T., and Møller, S. (2016). Indocyanine green retention test (icg-r15)
558 as a noninvasive predictor of portal hypertension in patients with different severity of cirrhosis. *European*
559 *journal of gastroenterology & hepatology* 28, 948–954. doi:10.1097/MEG.0000000000000611
- 560 Pugh, R. N., Murray-Lyon, I. M., Dawson, J. L., Pietroni, M. C., and Williams, R. (1973). Transection
561 of the oesophagus for bleeding oesophageal varices. *The British journal of surgery* 60, 646–649.
562 doi:10.1002/bjs.1800600817
- 563 Renner, E., Wietholtz, H., Huguenin, P., Arnaud, M. J., and Preisig, R. (1984). Caffeine: a model compound
564 for measuring liver function. *Hepatology (Baltimore, Md.)* 4, 38–46. doi:10.1002/hep.1840040107

- 565 Rubin, T. M., Heyne, K., Luchterhand, A., Bednarsch, J., W R Vondran, F., Polychronidis, G., et al. (2017).
566 Kinetic validation of the limax test during 10 000 intravenous , javax.xml.bind.jaxbelement@10fb8f50,
567 c-methacetin breath tests. *Journal of breath research* 12, 016005. doi:10.1088/1752-7163/aa820b
- 568 Sakka, S. G. (2018). Assessment of liver perfusion and function by indocyanine green in the perioperative
569 setting and in critically ill patients. *Journal of clinical monitoring and computing* 32, 787–796. doi:10.
570 1007/s10877-017-0073-4
- 571 Schuppan, D. and Afdhal, N. H. (2008). Liver cirrhosis. *Lancet (London, England)* 371, 838–851.
572 doi:10.1016/S0140-6736(08)60383-9
- 573 Seyama, Y. and Kokudo, N. (2009). Assessment of liver function for safe hepatic resection. *Hepatology
574 research : the official journal of the Japan Society of Hepatology* 39, 107–116. doi:10.1111/j.1872-034X.
575 2008.00441.x
- 576 Somogyi, E. T., Bouteiller, J.-M., Glazier, J. A., König, M., Medley, J. K., Swat, M. H., et al. (2015).
577 libroadrunner: a high performance sbml simulation and analysis library. *Bioinformatics* 31, 3315–3321
- 578 Soons, P. A., De Boer, A., Cohen, A. F., and Breimer, D. D. (1991). Assessment of hepatic blood flow in
579 healthy subjects by continuous infusion of indocyanine green. *British journal of clinical pharmacology*
580 32, 697–704
- 581 Stockmann, M., Lock, J. F., Riecke, B., Heyne, K., Martus, P., Fricke, M., et al. (2009). Prediction of
582 postoperative outcome after hepatectomy with a new bedside test for maximal liver function capacity.
583 *Annals of surgery* 250, 119–125. doi:10.1097/SLA.0b013e3181ad85b5
- 584 Sunagawa, Y., Yamada, S., Kato, Y., Sonohara, F., Takami, H., Inokawa, Y., et al. (2021). Perioperative
585 assessment of indocyanine green elimination rate accurately predicts postoperative liver failure in patients
586 undergoing hepatectomy. *Journal of hepatobiliary-pancreatic sciences* 28, 86–94. doi:10.1002/jhbp.833
- 587 Thomas, M. N., Weninger, E., Angele, M., Bösch, F., Pratschke, S., Andrassy, J., et al. (2015).
588 Intraoperative simulation of remnant liver function during anatomic liver resection with indocyanine
589 green clearance (limon) measurements. *HPB : the official journal of the International Hepato Pancreato
590 Biliary Association* 17, 471–476. doi:10.1111/hpb.12380
- 591 Urso, R., Blardi, P., and Giorgi, G. (2002). A short introduction to pharmacokinetics. *European review for
592 medical and pharmacological sciences* 6, 33–44
- 593 Vaubourdolle, M., Gufflet, V., Chazouillères, O., Giboudeau, J., and Poupon, R. (1991). Indocyanine
594 green-sulfobromophthalein pharmacokinetics for diagnosing primary biliary cirrhosis and assessing
595 histological severity. *Clinical chemistry* 37, 1688–1690
- 596 Virtanen, P., Gommers, R., Oliphant, T. E., Haberland, M., Reddy, T., Cournapeau, D., et al. (2020).
597 SciPy 1.0: Fundamental Algorithms for Scientific Computing in Python. *Nature Methods* 17, 261–272.
598 doi:10.1038/s41592-019-0686-2
- 599 Wakabayashi, H., Ishimura, K., Izuishi, K., Karasawa, Y., and Maeta, H. (2004). Evaluation of liver
600 function for hepatic resection for hepatocellular carcinoma in the liver with damaged parenchyma. *The
601 Journal of surgical research* 116, 248–252. doi:10.1016/j.jss.2003.09.015
- 602 Wheeler, H. O., Cranston, W. I., and Meltzer, J. I. (1958). Hepatic uptake and biliary excretion of
603 indocyanine green in the dog. *Proceedings of the Society for Experimental Biology and Medicine.
604 Society for Experimental Biology and Medicine (New York, N.Y.)* 99, 11–14

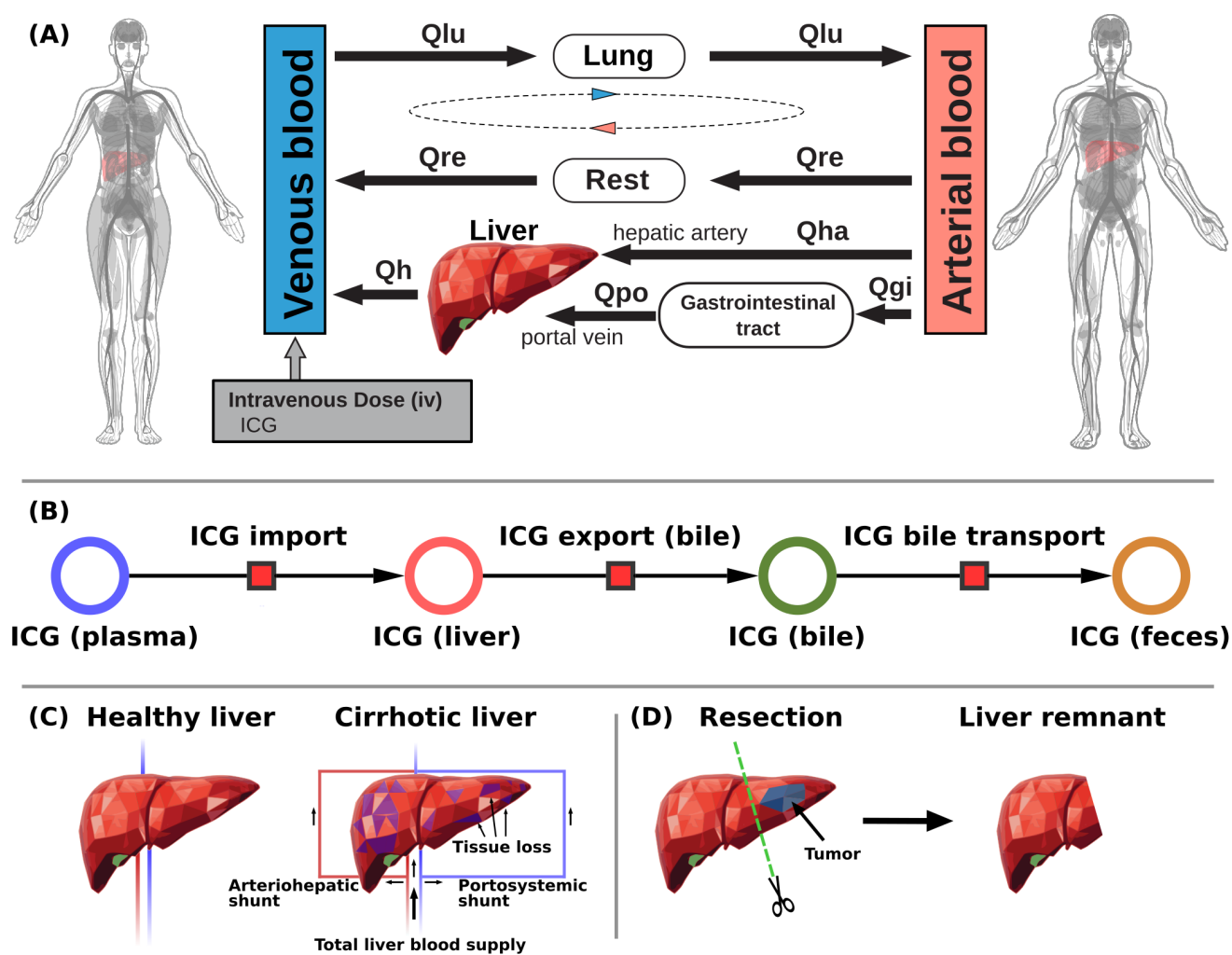


Figure 1. Model overview: **A:** Whole-body model. The whole-body PBPK model for ICG consists of venous blood, arterial blood, lung, liver, gastrointestinal tract and rest compartment (accounting for organs not modeled in detail) and the systemic blood circulation connecting these compartments. **B:** Liver model. ICG in the liver plasma compartment is taken up into the liver tissue (hepatocytes). Subsequently hepatic ICG is excreted in the bile from where it is excreted in the feces. No metabolism of ICG takes place in the liver. **C:** Modeling liver cirrhosis. Liver cirrhosis was modeled as a combination of tissue loss and hepatic shunts (see main text for details). **D:** Modeling hepatectomy. Hepatectomy was modeled as a removal of tissue volume with corresponding vessels (see main text for details)

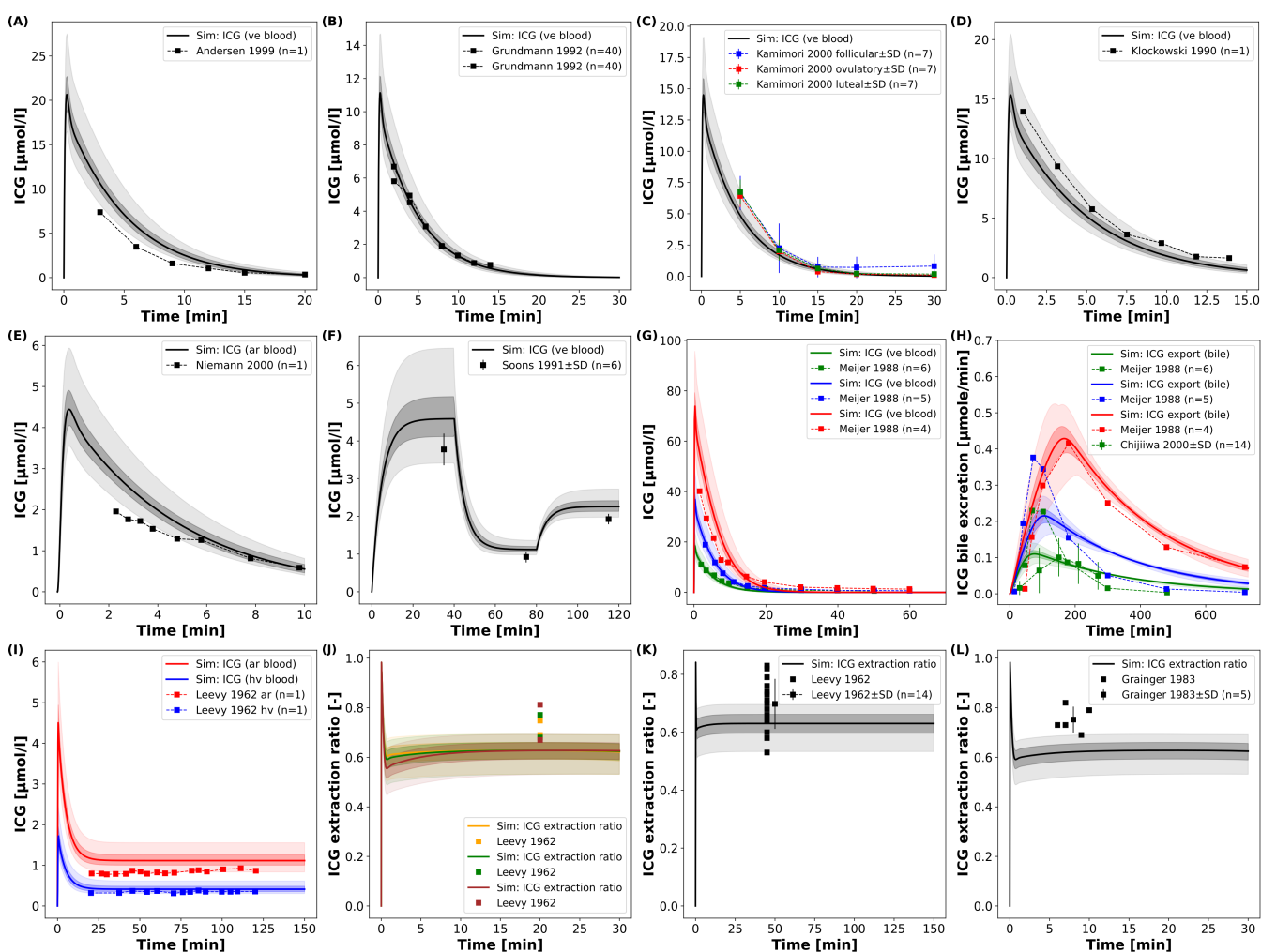


Figure 2. Model prediction of ICG time courses in healthy subjects: **A-D:** Venous concentration after bolus ICG administration (Andersen et al., 1999; Grundmann et al., 1992; Kamimori et al., 2000; Klockowski et al., 1990). **E:** Arterial concentration after bolus ICG administration (Niemann et al., 2000). **F:** Venous concentration during an ICG infusion protocol (2.0, 0.5, 1.0 mg/min, 40 minutes each) (Soons et al., 1991). **G, H:** Venous concentration and biliary excretion rate after 3 different ICG doses (0.5, 1.0, 2.0 mg/kg) (Meijer et al., 1988; Chijiwa et al., 2000). **I:** Hepatic venous and arterial concentration during constant ICG infusion (Leevy et al., 1962). **J-L:** ICG extraction ratio during constant infusion (Leevy et al., 1962; Grainger et al., 1983).

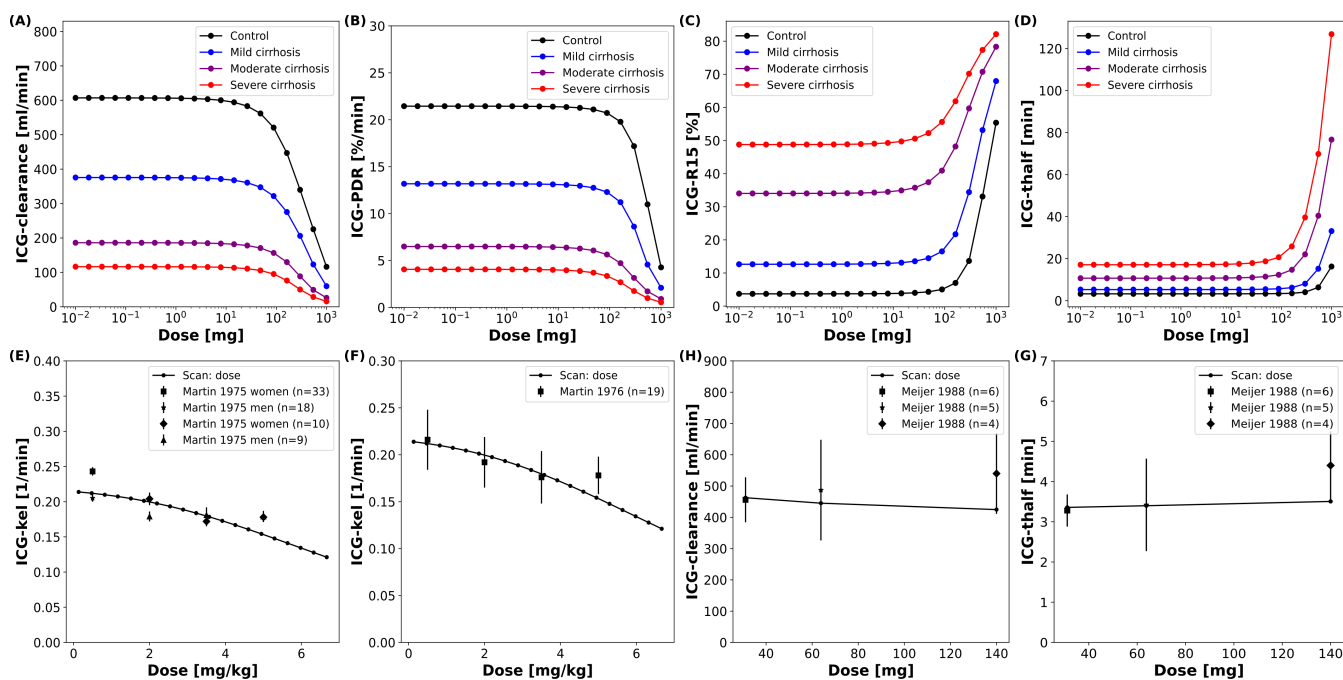


Figure 3. Dose dependency of ICG pharmacokinetic parameters: **A-D:** Dose dependency of ICG pharmacokinetic parameters in controls and three different degrees of cirrhosis. **E-H:** Dose dependency of ICG-kel, ICG-clearance, ICG-t_{1/2} in healthy subjects with clinical data (Martin et al., 1975, 1976; Meijer et al., 1988).

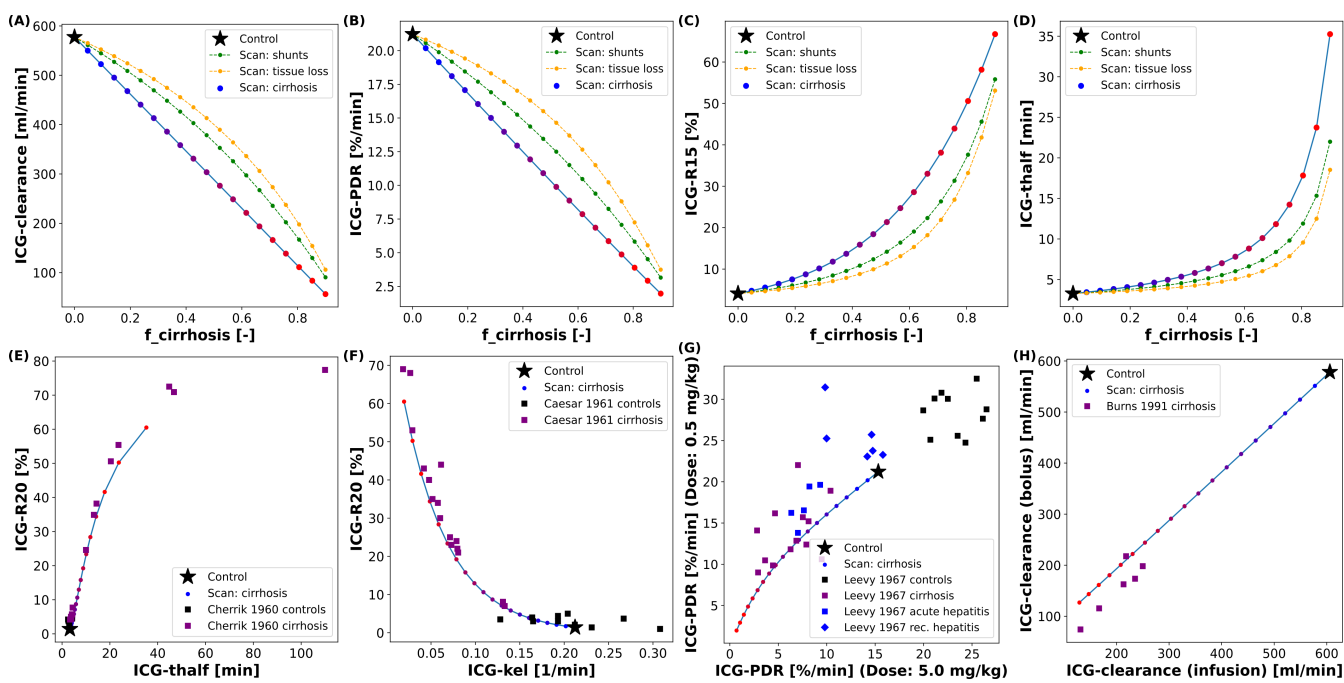


Figure 4. Dependency of ICG pharmacokinetic parameters on cirrhosis.: Simulation for healthy controls indicated by star. **A-D:** Dependency of ICG pharmacokinetic parameters on the degree of shunting (green), degree of tissue loss (yellow) and degree of cirrhosis (black-blue-red). **E:** Correlation between ICG-R20 and ICG- $t_{1/2}$ in cirrhotic and control subjects (Cherrick et al., 1960). **F:** Correlation between ICG-R20 and ICG-kel in cirrhotic and control subjects (Caesar et al., 1961). **G:** Correlation between ICG-PDR after an ICG dose of 0.5 mg/kg and 5.0 mg/kg in control subjects and subjects with various liver diseases (Leevy et al., 1967). **H:** Correlation between ICG-clearance after a bolus administration and during a constant infusion of ICG in cirrhotic subjects (Burns et al., 1991).

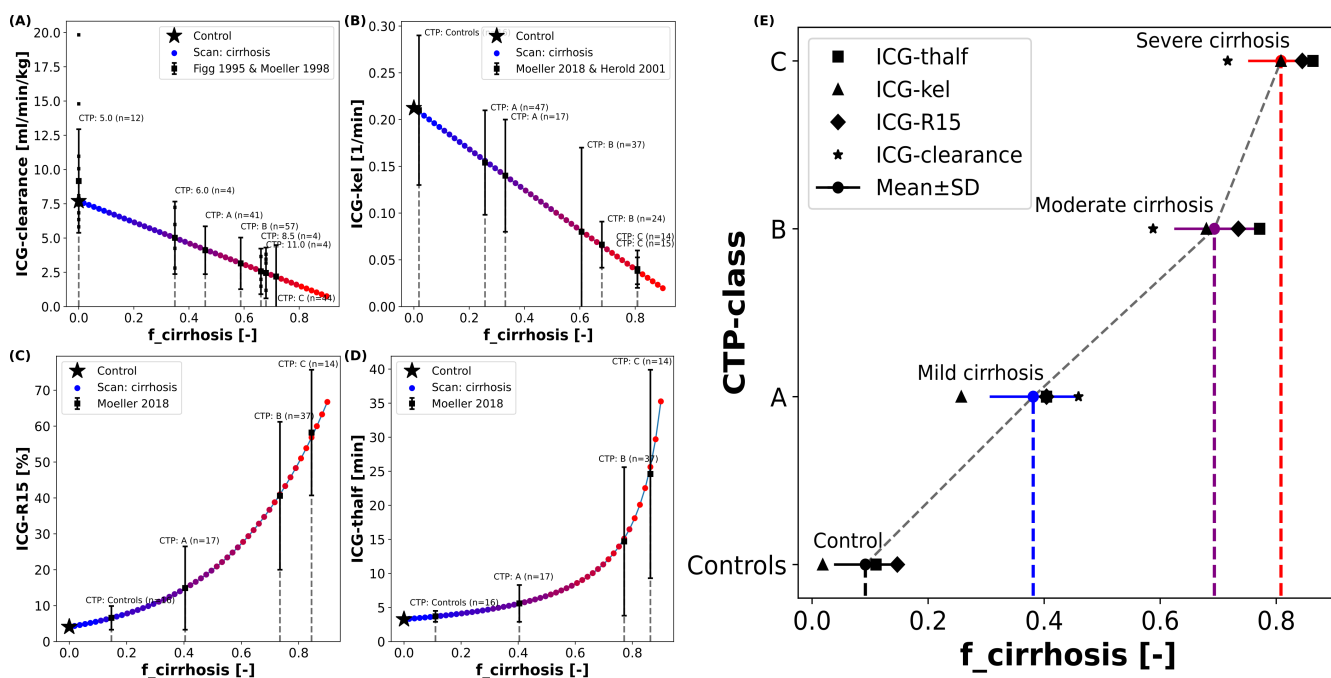


Figure 5. Mapping of model cirrhosis degree on CTP-score: **A:** Mapping based on ICG clearance (Figg et al., 1995; Møller et al., 1998). **B:** Mapping based on ICG-kel (Møller et al., 2019; Herold et al., 2001). **C:** Mapping based on ICG-R15 (Møller et al., 2019). **D:** Mapping based on ICG-thalf (Møller et al., 2019). **E:** Resulting $f_{cirrhosis}$ values for each CTP-class combining the information from the mappings based on individual ICG pharmacokinetic parameters (Control: $f_{cirrhosis} = 0.0$; Mild cirrhosis: 0.38; Moderate cirrhosis: 0.69; Severe cirrhosis: 0.81).

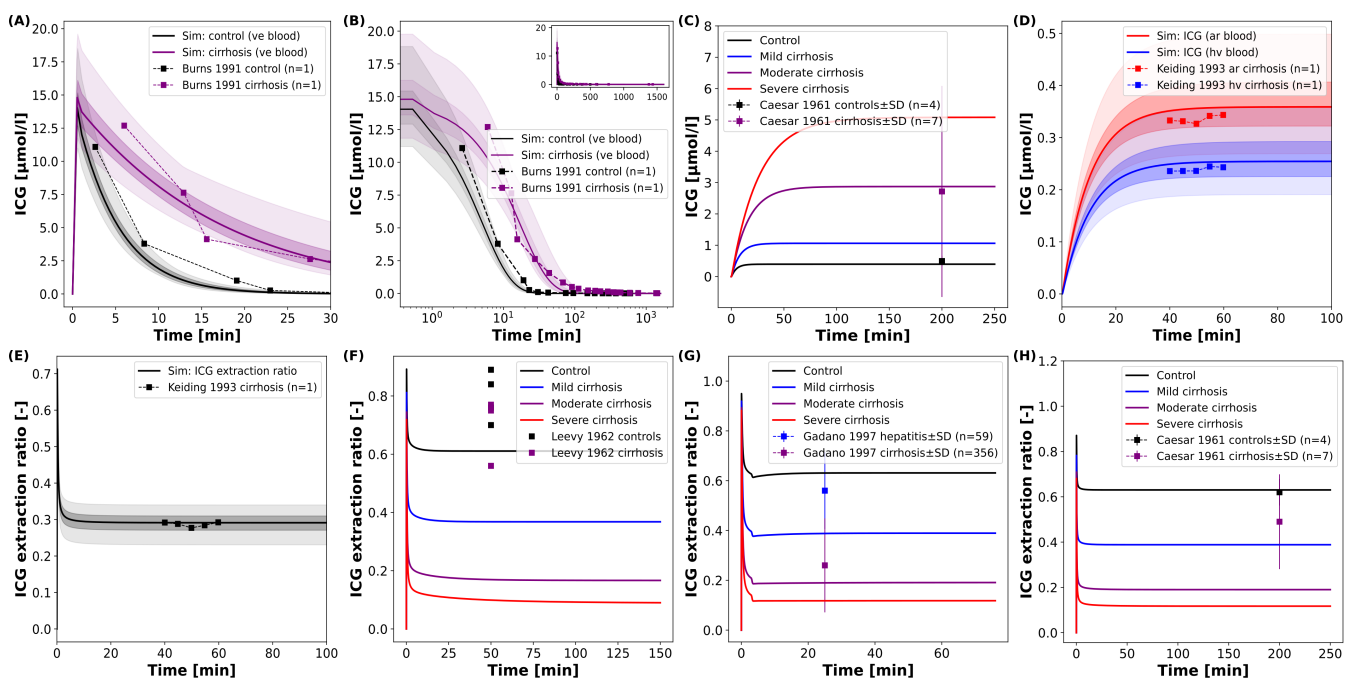


Figure 6. Model prediction of ICG time courses in subjects with cirrhosis: **A, B:** Venous concentration after a bolus ICG administration in a healthy subject and a cirrhotic patient ($f_{cirrhosis}$ was set to 0.7 corresponding to moderate cirrhosis) (Burns et al., 1991). **C:** Venous concentration during a constant ICG infusion in healthy and cirrhotic subjects (Caesar et al., 1961). **D, E:** Hepatic venous and arterial ICG concentration and ICG extraction ratio in a cirrhotic patient ($f_{cirrhosis}$ was set to 0.54 corresponding to mild-moderate cirrhosis) (Keiding et al., 1993). **F-H:** ICG extraction ratio in cirrhotic, hepatitis and control subjects during a constant ICG infusion (Leevy et al., 1962; Gadano et al., 1997; Caesar et al., 1961).

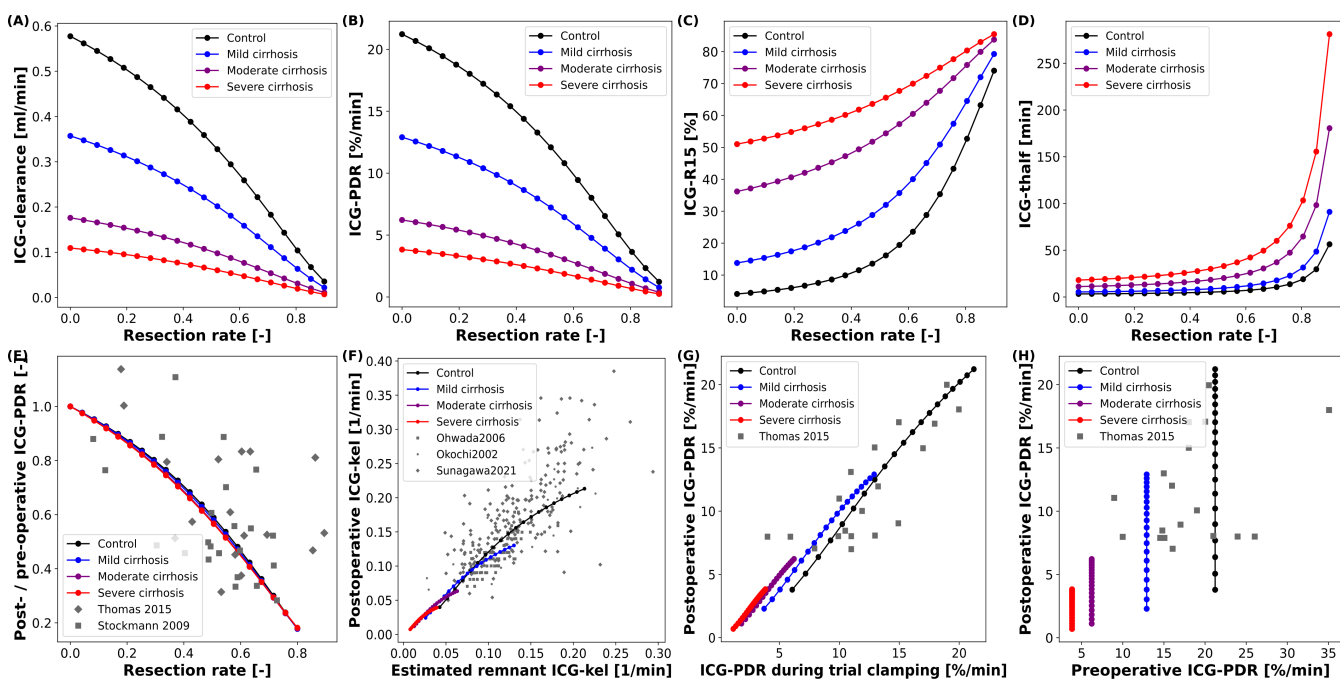


Figure 7. Model prediction of ICG pharmacokinetic parameters in hepatectomy under varying degree of cirrhosis: **A-D:** Dependency of postoperative ICG pharmacokinetic parameters on the resected volume in 4 different degrees of cirrhosis. **E:** Dependency of postoperative change in ICG-PDR on the resected volume (Thomas et al., 2015; Stockmann et al., 2009). **F:** Correlation between the measured postoperative ICG-kel and the estimated postoperative ICG-kel (product of preoperative ICG-kel and the future liver remnant) (Ohwada et al., 2006; Okochi et al., 2002; Sunagawa et al., 2021). **G:** Correlation between postoperative ICG-PDR and intraoperative ICG-PDR during trial clamping (Thomas et al., 2015). **H:** Correlation between postoperative and preoperative ICG-PDR (Thomas et al., 2015). Simulations for E-H: were performed for varying resection rates in healthy subjects and three different degrees of cirrhosis.

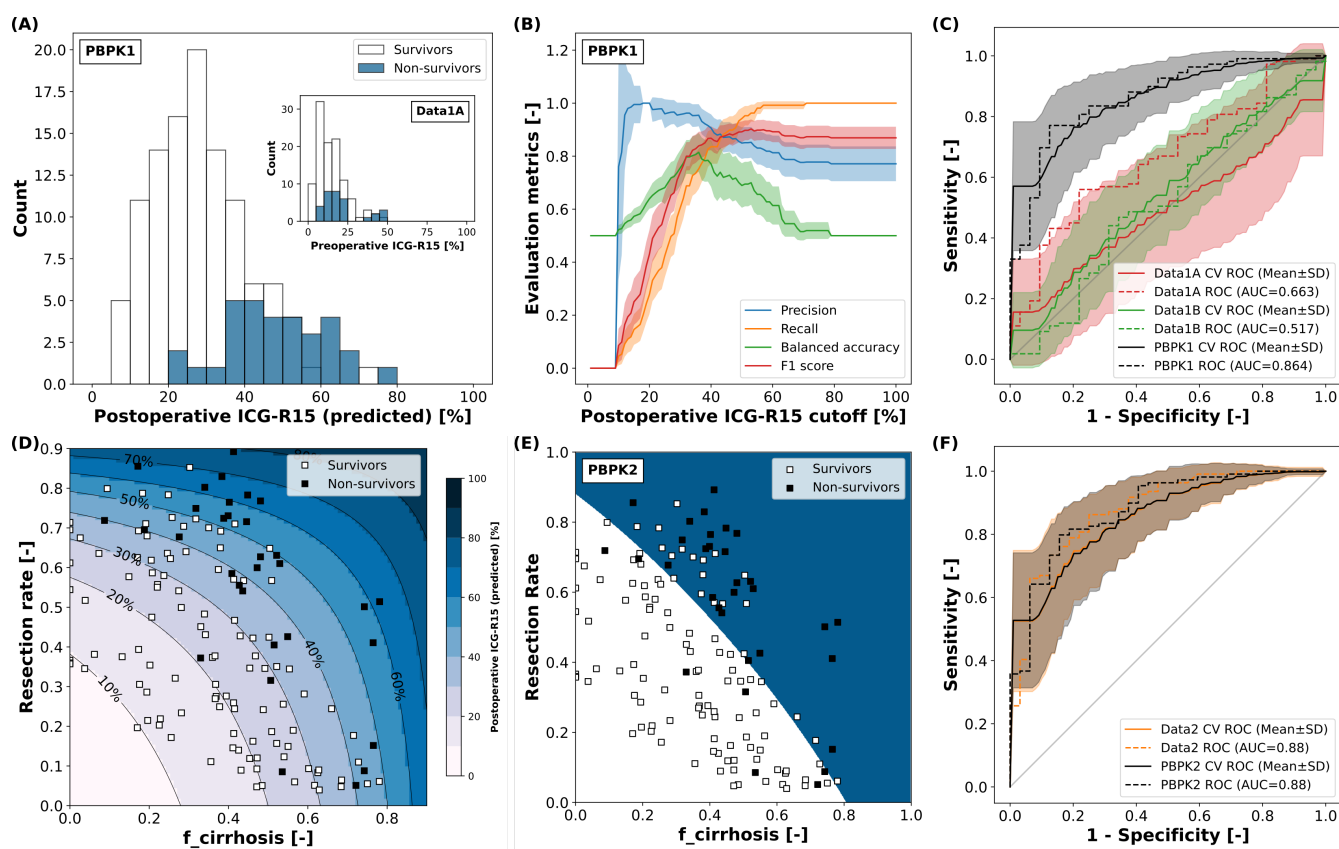


Figure 8. Classification of survival after hepatectomy: **A:** Distribution of predicted postoperative ICG-R15 in survivors and non-survivors based on the PBPK1 model. Corresponding measured preoperative ICG-R15 used in Data1A as inlet. **B:** Dependency of evaluation metrics of the classification model PBPK1 on the chosen cutoff of predicted postoperative ICG-R15 using cross-validation (mean \pm SD). **C:** ROC curve using the complete dataset ($n=141$) with cross-validation (mean \pm SD) for classification models Data1A, Data1B and PBPK1. **D:** Predicted postoperative ICG-R15 and survival status depending on the resection rate and $f_{cirrhosis}$. **E:** Decision boundary of the two-dimensional classification model PBPK2 based on the resection rate and $f_{cirrhosis}$ using the complete dataset. Survivors and non-survivors are well separated by the decision boundary. **F:** ROC curve using the complete dataset ($n=141$) with cross-validation (mean \pm SD) for classification models Data2 and PBPK2. Data from (Seyama and Kokudo, 2009; Wakabayashi et al., 2004).

Table 1. Overview of curated clinical studies.

Study	PK-DB	PMID	Protocol	Body weight	Fit	Data used in fit	Description
Andersen1999	PKDB00386	10499483	Bolus: 0.5 mg/kg	Contr.: 83.4 kg; Panc. 58.2 kg	✓	ICG time course (plasma)	Pharmacokinetic time course of ICG-disappearance in chronic pancreatitis and healthy subjects.
Burns1991	PKDB00388	1848168	Bolus: 0.5 mg/kg; Infusion: 0.25 mg/min	NR	✓	ICG time course (plasma)	ICG pharmacokinetics in healthy subjects and patients with liver disease.
Caesar1961	PKDB00389	13689739	Bolus: 0.5 mg/kg; Infusion: 0.5 mg/min	NR	✓	ICG extraction-ratio	Measuring hepatic blood flow and assessing hepatic function by ICG pharmacokinetics.
Cherrik1960	PKDB00390	13809697	Bolus: 0.5 mg/kg	NR	-	-	ICG pharmacokinetics in healthy subjects and patients with liver disease.
Chijiwa2000	PKDB00391	10773154	Bolus: 0.5 mg/kg	NR	✓	ICG time course (bile excretion)	Biliary excretion of ICG and ATP-dependency of ICG pharmacokinetics.
Figg1995	PKDB00393	8602375	Bolus: 0.5 mg/kg	NR	-	-	Comparison of methods to assess hepatic function including CTP-score and ICG-clearance
Gadano1997	PKDB00394	9083919	Infusion: 0.4 mg/min (controls); 0.8 mg/min (cirrhotics) with priming dose (24 mg controls; 12 mg cirrhotics).	NR	✓	-	ICG-clearance and extraction-ratio and their dependency on hepatic bloodflow in healthy subjects and in patients of hepatic fibrosis and cirrhosis.
Grainger1983	PKDB00395	6822056	Bolus: 0.25 mg/kg	NR	✓	ICG extraction-ratio	Non-invasive measurement of hepatic blood flow using ICG extraction-ratio.
Grundmann1992	PKDB00396	1482735	Bolus: 0.3 mg/kg	NR	✓	ICG time course (plasma)	Effect of anesthetics on ICG-pharmacokinetics and hepatic blood flow.
Herold2001	PKDB00397	11169069	Bolus: 0.5 mg/kg	NR	-	-	Comparison of liver function tests. Correlation between CTP-score and ICG-kel in healthy subjects and cirrhotic patients.
Kamimori2000	PKDB00299	10883415	Bolus: 0.5 mg/kg	58.6 ± 11.2 kg	✓	ICG time course (plasma)	Effect of the menstrual cycle on ICG pharmacokinetics.
Keiding1993	PKDB00402	8151094	Infusion: 0.08 mg/min	NR	-	-	Effect of changing plasma protein concentrations on ICG-extraction.
Klockowski1990	PKDB00403	2146057	Bolus: 0.5 mg/kg	NR	✓	ICG time course (plasma)	Effect of isradipine and diltiazem on ICG-pharmacokinetics.
Leevy1962	PKDB00404	14463639	Infusion: 0.3 and 1.5 mg/min/m ² with priming dose (10 mg).	NR	✓	ICG extraction-ratio; ICG time course (hv and ar)	Estimation of hepatic blood flow using ICG.
Leevy1967	PKDB00405	6071462	Bolus: 0.5 mg/kg and 5.0 mg/kg	NR	-	-	Estimation of liver function with ICG. Dose dependency of ICG-PDR.
Martin1975	PKDB00406	1208580	Bolus: 0.5, 2.0, 3.5 and 5.0 mg/kg	NR	-	-	Differences in ICG-pharmacokinetics in men and women at varying ICG-doses.
Martin1976	PKDB00407	814028	Bolus: 0.5, 2.0, 3.5 and 5.0 mg/kg	NR	-	-	ICG-pharmacokinetics in patients with Gilbert's Syndrome.
Meijer1988	PKDB00408	3181282	Bolus: 0.5, 1.0 and 2.0 mg/kg	64.8 kg	✓	ICG time course (plasma and bile excretion)	Biliary excretion of ICG at different doses.
Moeller1998	PKDB00409	9691928	Infusion: Rate not reported	72.7 (40-115) kg	-	-	Arterial hypoxaemia in cirrhosis. Correlation between ICG-clearance and CTP-score.
Moeller2019	PKDB00410	30221390	Infusion: 0.2 mg/min with priming dose (2 mg), Bolus: 0.5 mg/kg	79.2 ± 18.5 kg	-	-	Correlation between ICG-pharmacokinetics and CTP-score.
Niemann2000	PKDB00414	10801242	Bolus: 10 mg	80 ± 17 kg	✓	ICG time course (plasma)	ICG- pharmacokinetic time course under administration of propranolol.
Ohwada2006	PKDB00412	16498606	Bolus: 20 mg	NR	-	-	Prediction of postoperative liver functional capacity based on ICG-pharmacokinetics.
Okochi2002	PKDB00415	11855925	Bolus: 20 mg	NR	-	-	Comparison of preoperative and postoperative ICG-pharmacokinetics. Prediction of postoperative liver functional capacity based on ICG-pharmacokinetics.
Seyama2009	PKDB00416	19208031	Bolus: 0.5 mg/kg	NR	-	-	Assessment of liver function for safe hepatic resection. Prediction of survival after hepatectomy based on ICG-R15.
Soons1991	PKDB00411	1768562	Infusion: 2.0, 0.5, 1.0 mg/min (consecutive)	72 ± 6 kg	✓	ICG time course (plasma)	Assessment of hepatic blood flow in healthy subjects by continuous infusion of ICG.
Stockmann2009	PKDB00417	19561474	Bolus: 0.5 mg/kg	NR	-	-	Prediction of postoperative liver functional capacity based on ICG-pharmacokinetics.
Sunagawa2021	PKDB00418	33052632	Bolus: 20 mg	NR	-	-	Prediction of postoperative liver failure based on ICG-kel measurements.
Thomas2015	PKDB00419	25581073	Bolus: 0.25 mg/kg	NR	-	-	Intraoperative prediction of postoperative liver functional capacity using trial-clamping and ICG-pharmacokinetics.
Wakabayashi2004	PKDB00420	15013363	Bolus: 0.5 mg/kg	NR	-	-	Correlation between preoperative ICG-R15 and estimated liver remnant. Prediction of survival based on ICG-R15.

Table 2. Overview of key model parameters.

Parameter	Description	Value	Unit	Fitted
<i>BW</i>	Body weight	75	kg	-
<i>COBW</i>	Cardiac output per body weight	0.83	ml/s/kg	-
<i>QC</i>	Cardiac output (<i>BW</i> · <i>COBW</i>)	3.75	l/min	-
<i>HCT</i>	Hematocrit	0.51	-	-
<i>Fblood</i>	Fraction of organ volume that is blood vessels	0.02	-	-
<i>FVgi</i>	Fractional tissue volume gastrointestinal tract	0.0171	l/kg	-
<i>FVli</i>	Fractional tissue volume liver	0.0210	l/kg	-
<i>FVlu</i>	Fractional tissue volume lung	0.0076	l/kg	-
<i>FVve</i>	Fractional tissue volume venous blood	0.0587	l/kg	-
<i>FVar</i>	Fractional tissue volume arterial blood	0.0184	l/kg	-
<i>LI_ICGIM_Vmax</i>	<i>V_{max}</i> of liver import	2.25E-2	mmole/min/l	✓
<i>LI_ICGIM_Km</i>	<i>K_m</i> of liver import	1.39E-2	mM	✓
<i>LI_ICGLI2CA_Vmax</i>	<i>V_{max}</i> of bile excretion	9.58E-4	mmole/min/l	✓
<i>LI_ICGLI2CA_km</i>	<i>K_m</i> of bile excretion	1.18E-2	mM	✓
<i>LI_ICGLI2BI_Vmax</i>	<i>V_{max}</i> of bile transport	1.14E-4	1/min	✓

Table 3. Evaluation metrics for classification models of survival after hepatectomy. Evaluation metrics of classification model are values for the model fitted with the complete dataset. . Mean ± SD of cross validation reported in brackets.

Classification Model Features	Data1A Preoperative ICG-R15	Data1B Postoperative ICG-R15 (calculated)	PBPK1 Postoperative ICG-R15 (predicted)	Data2 Preoperative ICG-R15 & Resection rate	PBPK2 <i>f_{cirrhosis}</i> & Resection rate
ROC AUC	0.663 (0.656 ± 0.096)	0.517 (0.445 ± 0.1)	0.864 (0.863 ± 0.072)	0.88 (0.858 ± 0.077)	0.88 (0.858 ± 0.076)
Accuracy	0.562 (0.555 ± 0.072)	0.515 (0.481 ± 0.052)	0.788 (0.765 ± 0.089)	0.785 (0.767 ± 0.09)	0.81 (0.767 ± 0.09)
F1-score	0.861 (0.852 ± 0.048)	0.85 (0.722 ± 0.279)	0.87 (0.86 ± 0.05)	0.851 (0.847 ± 0.047)	0.867 (0.841 ± 0.052)
Precision	0.797 (0.792 ± 0.067)	0.779 (0.7 ± 0.194)	0.918 (0.906 ± 0.056)	0.925 (0.912 ± 0.056)	0.936 (0.915 ± 0.054)
Recall	0.936 (0.927 ± 0.053)	0.936 (0.793 ± 0.322)	0.826 (0.823 ± 0.075)	0.789 (0.795 ± 0.072)	0.807 (0.783 ± 0.081)

SUPPLEMENTAL FIGURES

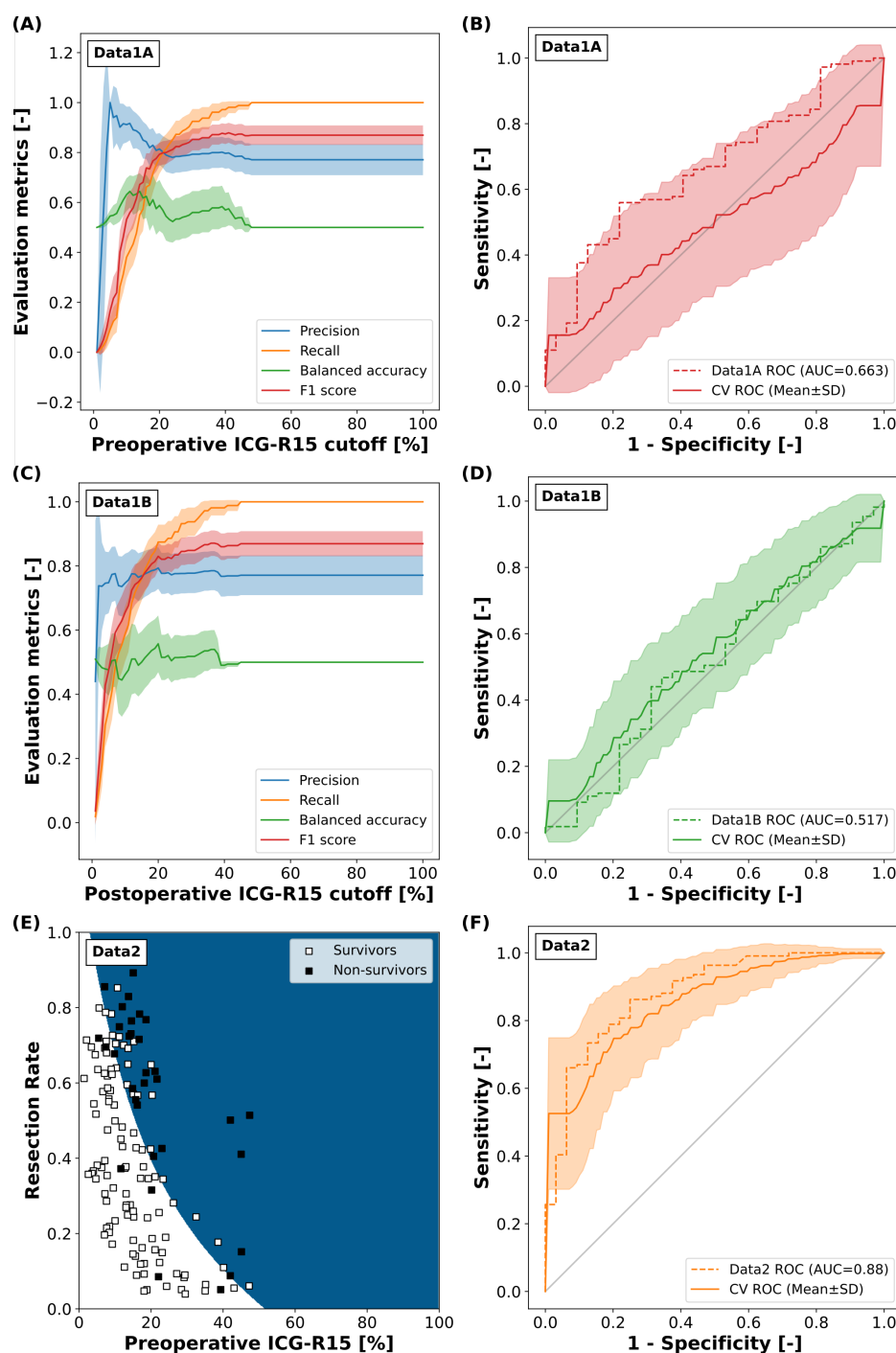


Figure 9. Classification of survival after hepatectomy: **A:** Dependency of evaluation metrics of the classification model Data1A on the chose cutoff of preoperative ICG-R15 using cross-validation (mean \pm SD). **B:** ROC curve using the complete dataset ($n=141$) with cross-validation (mean \pm SD) for classification model Data1A. **C:** Dependency of evaluation metrics of the classification model Data1B on the chose cutoff of preoperative ICG-R15 using cross-validation (mean \pm SD). **D:** ROC curve using the complete dataset ($n=141$) with cross-validation (mean \pm SD) for classification model Data1B. **E:** Decision boundary of the two-dimensional classification model Data2 based on the resection rate and the preoperative ICG-R15 using the complete dataset. **F:** ROC curve using the complete dataset ($n=141$) with cross-validation (mean \pm SD) for classification model Data2.